

1

High-frequency variability in the

2

North Icelandic Jet

3

B. E. Harden¹ and R. S. Pickart

4

Woods Hole Oceanographic Institution, Woods Hole, USA

5

January 25, 2018

¹Woods Hole Oceanographic Institution, 266 Woods Hole Road, Woods Hole, MA 02543.
bharden@whoi.edu

ABSTRACT

7 We describe the high-frequency variability in the North Icelandic Jet (NIJ) on the Iceland
8 Slope using data from the densely instrumented Kögur mooring array deployed upstream
9 of the Denmark Strait sill from September 2011 to July 2012. Significant sub-8-day vari-
10 ability is ubiquitous in all moorings from the Iceland slope with a dominant period of
11 3.6 days. We attribute this variability to topographic Rossby waves on the Iceland slope
12 with a wavelength of 62 ± 3 km and a phase velocity of 17.3 ± 0.8 km day⁻¹ directed
13 downslope (-9°T). We test the theoretical dispersion relation for these waves against our
14 observations and find good agreement between the predicted and measured direction of
15 phase propagation. We additionally calculate a theoretical group velocity of 36 km day⁻¹
16 directed almost directly up-slope (138°T) which agrees well with the propagation speed
17 and direction of observed energy pulses. We use an inverse wave tracing model to show
18 that this wave energy is generated locally, offshore of the array, and does not emanate
19 from the upstream or downstream directions along the Iceland slope. It is hypothesized
20 that either the meandering Separated East Greenland Current located seaward of the NIJ,
21 or intermittent aspiration of dense water into the Denmark Strait Overflow, are the drivers
22 of the topographic waves.

23 **1. Introduction**

24 The Denmark Strait Overflow is the major pathway of dense water out of the Nordic
25 Seas. It transports 3.2 Sv, or approximately 50%, of the total outflow (Dickson and Brown,
26 1994; Jochumsen *et al.*, 2017), and hence plays a crucial role in the Atlantic meridional
27 overturning circulation (AMOC). While the existence of this overflow has been known
28 for many decades, our understanding of the processes that govern it and the underlying
29 dynamics remains incomplete. One important aspect that requires further study is deter-
30 mining the upstream sources of the dense water and how it approaches the sill. If we are to
31 determine how a changing climate might impact the AMOC, we need to understand bet-
32 ter the connection between the water mass transformation process and the flux of newly
33 ventilated water to Denmark Strait.

34 Most of the Denmark Strait Overflow water (approximately 70%) comes from the
35 East Greenland Current by way of the Nordic Seas boundary current system (Våge *et al.*,
36 2013; Harden *et al.*, 2016) (see Figure 1). Specifically, warm Atlantic inflow across the
37 Greenland-Scotland Ridge is progressively cooled as it flows northward towards Fram
38 Strait, much of it recirculating in the strait and subducting to mid-depth (Mauritzen, 1996).
39 This is joined by Atlantic water exiting the strait that has circumnavigated the Arctic, and
40 together the transformed Atlantic water flows southward in the East Greenland Current.
41 As the current rounds Scoresby Sund, it splits into two branches (Figure 1). One continues
42 towards the sill as a shelfbreak jet (Håvik *et al.*, 2017). The other carries approximately
43 60% of the East Greenland Current water out into the central strait via eddies and/or gyre-
44 like deflections of the shelfbreak jet (Våge *et al.*, 2013; Harden *et al.*, 2016). This interior
45 pathway, known as the separated East Greenland current, then flows into the strait along
46 the outer Iceland slope.

47 The remaining 30% of Denmark Strait Overflow water is supplied by the North Ice-
48 landic Jet (NIJ), a more recently discovered branch of the upstream circulation (Jonsson
49 and Valdimarsson, 2004; Våge *et al.*, 2011). This mid-depth intensified jet advects waters

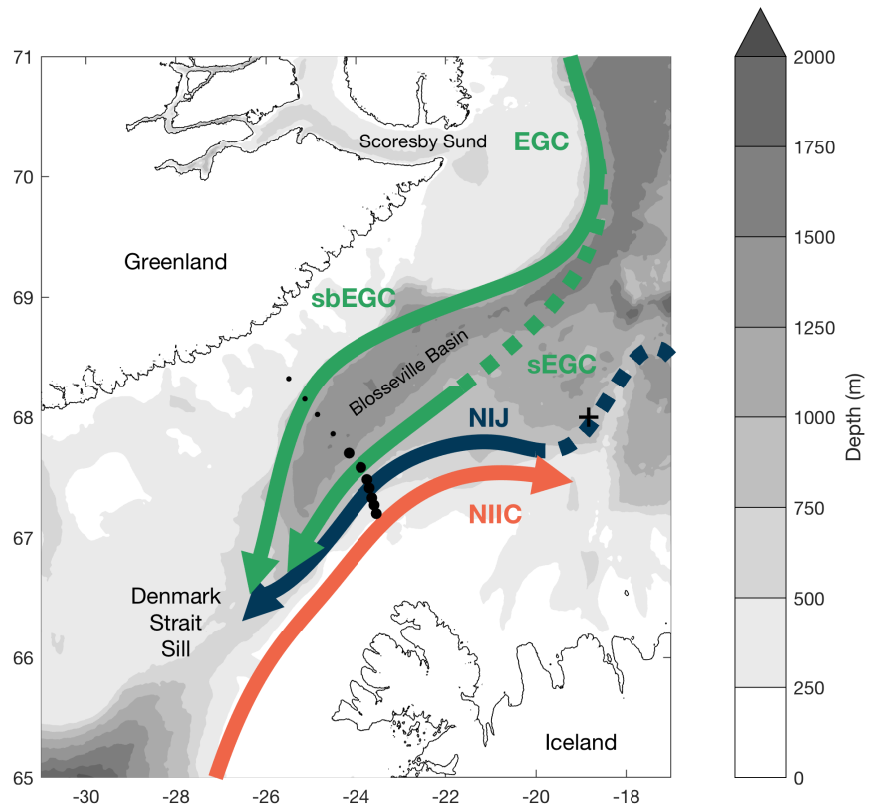


Figure 1: Map of the study region showing the overflow pathways approaching the Denmark Strait Sill: the North Icelandic Jet (NIJ) and the two East Greenland Current (EGC) pathways, one along the shelfbreak (sbEGC) and the other in a separated branch on the Iceland Slope (sEGC). Dashed portions show parts of pathways that still need further clarification. Also shown is the northward flowing surface-intensified current, the North Icelandic Irminger Current (NIIC). Black dots show the locations of the moorings in the Kögur array with larger dots indicating the subset of seven moorings used in this study. The upstream cross is the mooring to the west of the Kolbensey ridge referred to in the text. The bathymetry is from IBCAO v3.

50 distinct from those found in the East Greenland Current (colder and fresher) suggestive of
51 a source in the central Iceland or Greenland seas (Våge *et al.*, 2011; 2015; Harden *et al.*,
52 2016). The NIJ contains the densest water that feeds the overflow; its waters are found in
53 the deepest part of the sill (Mastropole *et al.*, 2017) and subsequently sink to the deepest
54 depths in the core of the overflow.

55 The leading hypothesis for the formation of the NIJ, supported by both models and
56 observations, is that it represents the lower limb of a local overturning cell in the Iceland
57 sea (Våge *et al.*, 2011; Behrens *et al.*, 2017). The upper limb of the cell is the NIIC, which
58 sheds warm water into the Iceland Sea that is cooled by air-sea heat loss. The transformed
59 water then returns southward towards the boundary where it sinks and forms the NIJ.
60 However, many questions remain unanswered about this proposed system. For instance,
61 the winter mixed-layers in the Iceland Sea don't appear to be dense enough to account for
62 the deepest water in the NIJ (Våge *et al.*, 2015), whereas those in the Greenland Sea do
63 (Strass *et al.*, 1993; Rudels *et al.*, 2002).

64 Regardless of the source of the NIJ, it clearly constitutes a vital component of the
65 circulation upstream of the sill. Harden *et al.* (2016) investigated the jet's mean and sea-
66 sonal contribution to the overflow, demonstrating that there is time-dependent partitioning
67 of transport between the NIJ and the other two overflow branches on weekly to monthly
68 timescales, likely driven by the wind. Pickart *et al.* (2017) noted that the NIJ appears to
69 be coupled to the northward-flowing NIIC and that, on occasion, it consists of multiple
70 branches. Using historical hydrographic data, Pickart *et al.* (2017) also revealed a clear
71 link between the interannually varying properties of the NIJ and those of the densest water
72 at the Denmark Strait sill, leaving little doubt that the NIJ is a major source of the overflow
73 plume.

74 It has long been known that the Denmark Strait Overflow varies on short (order days)
75 timescales (Smith, 1976; Bruce, 1995; Käse *et al.*, 2003). Some of this variability is
76 associated with the passage of lenses of cold, dense, overflow water referred to as boluses

77 (Cooper, 1955). Recently, von Appen *et al.* (2017) identified a second type of mesoscale
78 feature in the strait that was termed a pulse. In contrast to boluses, pulses correspond to
79 a thinning of the overflow layer associated with a large increase in equatorward velocity.
80 Both of these features have been identified in a high-resolution regional model as well
81 (Almansi *et al.*, 2017). von Appen *et al.* (2017) showed that, taking into account both
82 boluses and pulses, a mesoscale feature passes through Denmark Strait on average every
83 2 days. Presently, however, it is unknown if these disturbances originate from upstream or
84 if they are associated with local dynamics near the sill.

85 The goal of the present study is to shed light on some of the above processes by de-
86 scribing the high frequency variability of the NIJ north of the Denmark Strait. We use
87 timeseries data from a year-long mooring array that was maintained roughly 200 km up-
88 stream of the sill (Figure 1). This is the same data set used by Harden *et al.* (2016) to inves-
89 tigate the mean and seasonal attributes of the NIJ. While Harden *et al.* (2016) mentioned
90 that the NIJ exhibits high-frequency variability, they did not elaborate on this. We begin
91 with a brief description of the data, followed by a characterization of the high-frequency
92 signal. We discuss how this signal is consistent with the existence of topographic Rossby
93 waves on the Iceland slope, and then investigate the source region of the energy in these
94 waves through inverse wave tracing.

95 **2. Data and Methods**

96 The data for this study come from the densely instrumented Kögur mooring array
97 spanning the Denmark Strait approximately 200 km upstream of the sill. The array was
98 deployed for 11 months from September 2011 to July 2012 and consisted of 12 moorings
99 (named KGA 1-12) equipped with instrumentation to measure both the hydrography and
100 velocity of the water column from 50 m to the bottom. Harden *et al.* (2016) present a
101 detailed description of the mooring data, including the instrumentation, processing steps,
102 and sensor accuracies. The array captured the majority of the overflow water (denser than

103 27.8 kg m⁻³) passing through the northern part of the strait towards the sill.

104 Here we use primarily the gridded product described in Harden *et al.* (2016), which
105 has a lateral resolution of 8km and vertical resolution of 50 m. Because of our focus
106 on the Iceland slope, we consider a subset of these data up to and including the location
107 of mooring KGA 7, approximately 70 km offshore of the Iceland shelfbreak. The mean
108 velocity sections demonstrate that this portion of the array captures both the NIJ and the
109 majority of the Separated EGC (Figure 2). For parts of the analysis we also use the data
110 on a mooring-by-mooring basis. All of the velocities have been de-tided using a 36-hour
111 low-pass filter.

112 Additional data come from a mooring located approximately 200 km upstream of the
113 Kögur Array on the west side of the Kolbesney Ridge (68°00'N, 18°50'W, see Figure
114 1) This was deployed on the 1000 m isobath from September 2007 to mid-October 2008
115 and consisted of a McLane Moored Profiler and acoustic current meter providing profiles
116 between 100 m and the bottom at 8 hour intervals. As with the Kögur data, we low-passed
117 the velocity timeseries using a 36-hr filter to remove the tidal components of the flow.
118 These data are described in greater detail by Jónsson and Valdimarsson (2012).

119 The inverse wave tracing of topographic Rossby waves (TRWs) was done using the
120 model described by Meinen *et al.* (1993) and implemented by Pickart (1995) for investigat-
121 ing TRWs in the Deep Western Boundary Current off of Cape Hatteras, North Carolina.
122 The method uses the TRW dispersion relation to calculate the group velocity and then
123 backtracks the evolution of the wave with a time step of 30 minutes. The wave parameters
124 are recalculated at each step for the local bottom depth, bottom slope, and water column
125 stratification. A new group velocity is then found and used to further trace the wave. Most
126 of the required input parameters for the inverse wave tracing model come directly from the
127 moored data and are the same as those used for the theoretical TRW dispersion relation
128 calculations (see Section 3.a.). For the bathymetry we used the International Bathymetric
129 Chart of the Arctic Ocean 30-arcsec gridded product (Jakobsson *et al.*, 2012). To remove

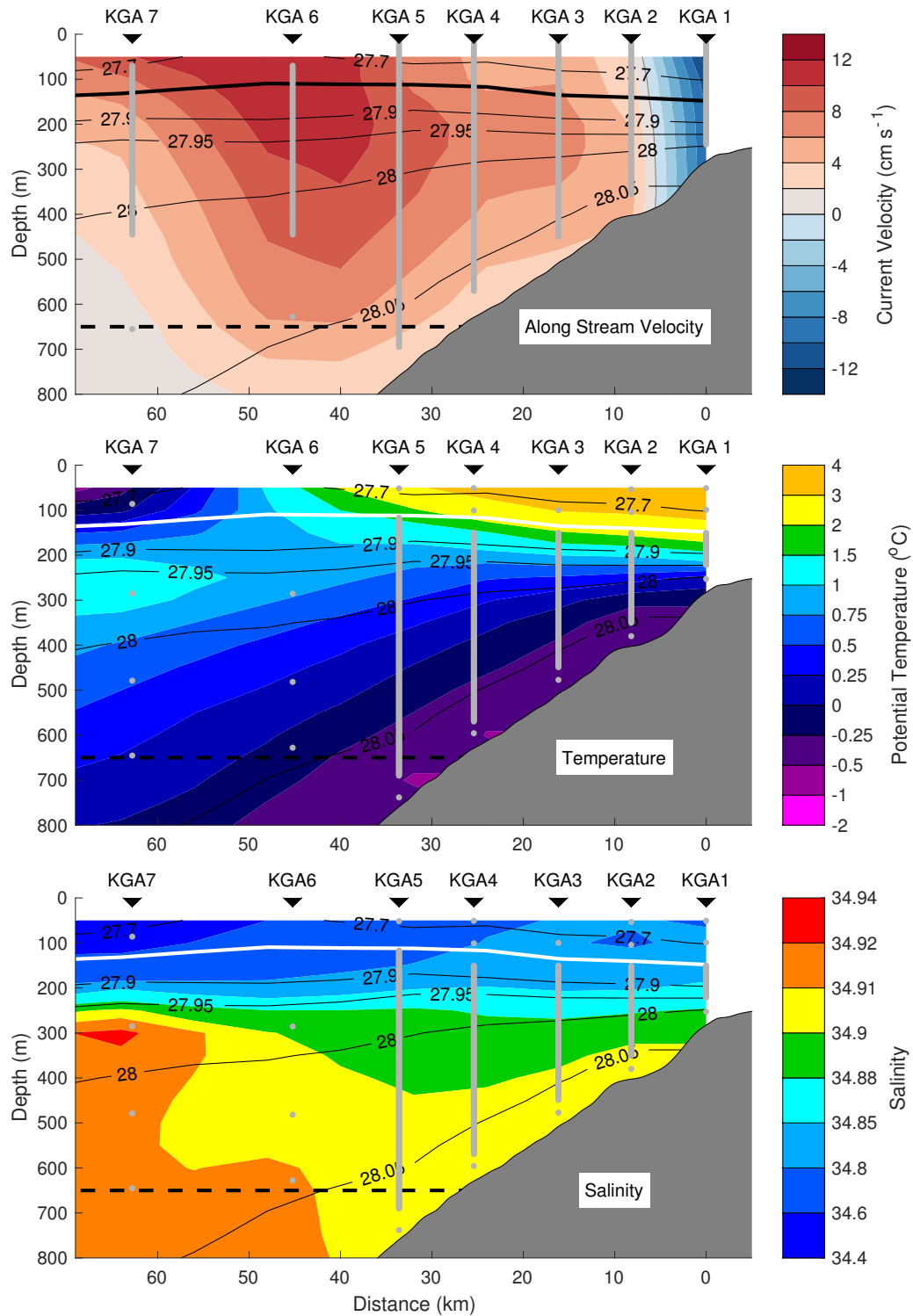


Figure 2: Mean vertical section of the along-stream (cross-transect) velocity (top), and median sections of potential temperature (middle) and salinity (bottom) for the 11-month period of the Kögur array. Overlaid in black contours on each panel is the mean density with the 27.8 kg m^{-3} isopycnal (the upper boundary of Denmark Strait Overflow Water) highlighted. The viewer is looking to the northeast with Iceland on the right. Positive velocities are equatorward. The horizontal black dashed line indicates the depth of the Denmark Strait sill. The moorings (black triangles) are labeled, and the average instrument locations are shown by the grey points. The bathymetry is from a shipboard echosounder.

130 seamounts and other sharp topographic features we smoothed the bathymetry using a filter
131 of 60 km (comparable to our measured TRW wavelength). In contrast to Pickart (1995)
132 who subsequently fit splines to the data to be able to find the bottom depth and gradients
133 at any location, we deemed our resolution to be high enough (and our smoothing window
134 great enough) to simply use linear interpolation. The total integration period for the wave
135 tracing was 48 hours.

136 **3. Results**

137 As discussed in Harden *et al.* (2016), the vertical sections of velocity and hydrography
138 at the Kögur site show the signatures of both the NIJ and the Separated EGC. However, the
139 two features are merged to some degree in the mean (Figure 2). The NIJ is on the upper
140 Iceland slope and is characterized by a mid-depth intensified flow carrying the coldest,
141 densest overflow water banked up on the slope. The Separated EGC is farther offshore;
142 its key features are a surface intensification and the transport of warmer, saltier overflow
143 water at approximately 300 m. Inshore of both these currents, on the Iceland shelf, is the
144 poleward flowing NIIC (see also Figure 1).

145 The two overflow currents are merged in the mean largely due to the high degree
146 of variability on weekly timescales. The depth-integrated, along-stream velocity exhibits
147 constant pulsing through this portion of the strait (Figure 3a). The period of the pulsing
148 in the vicinity of the NIJ is concentrated at sub-8-day periods with a maximum average
149 energy at 3.6 days (Figure 4). Farther offshore, near the Separated EGC, we also see
150 such short-period pulses in addition to more consistent longer-period variability (Figure
151 3a). The lower frequency signals were described by Harden *et al.* (2016) and attributed in
152 part to the time-varying upstream bifurcation of the EGC. Here we focus on the higher-
153 frequency, sub-8-day variability. To facilitate this we used an 8-day butterworth filter.¹

154 The current ellipses of this high-frequency variability for each mooring are useful for

¹Different period filters were implemented, ranging in length from 4 days to 30 days, but the 8-day filter was most effective in isolating the peak high-frequency energy.

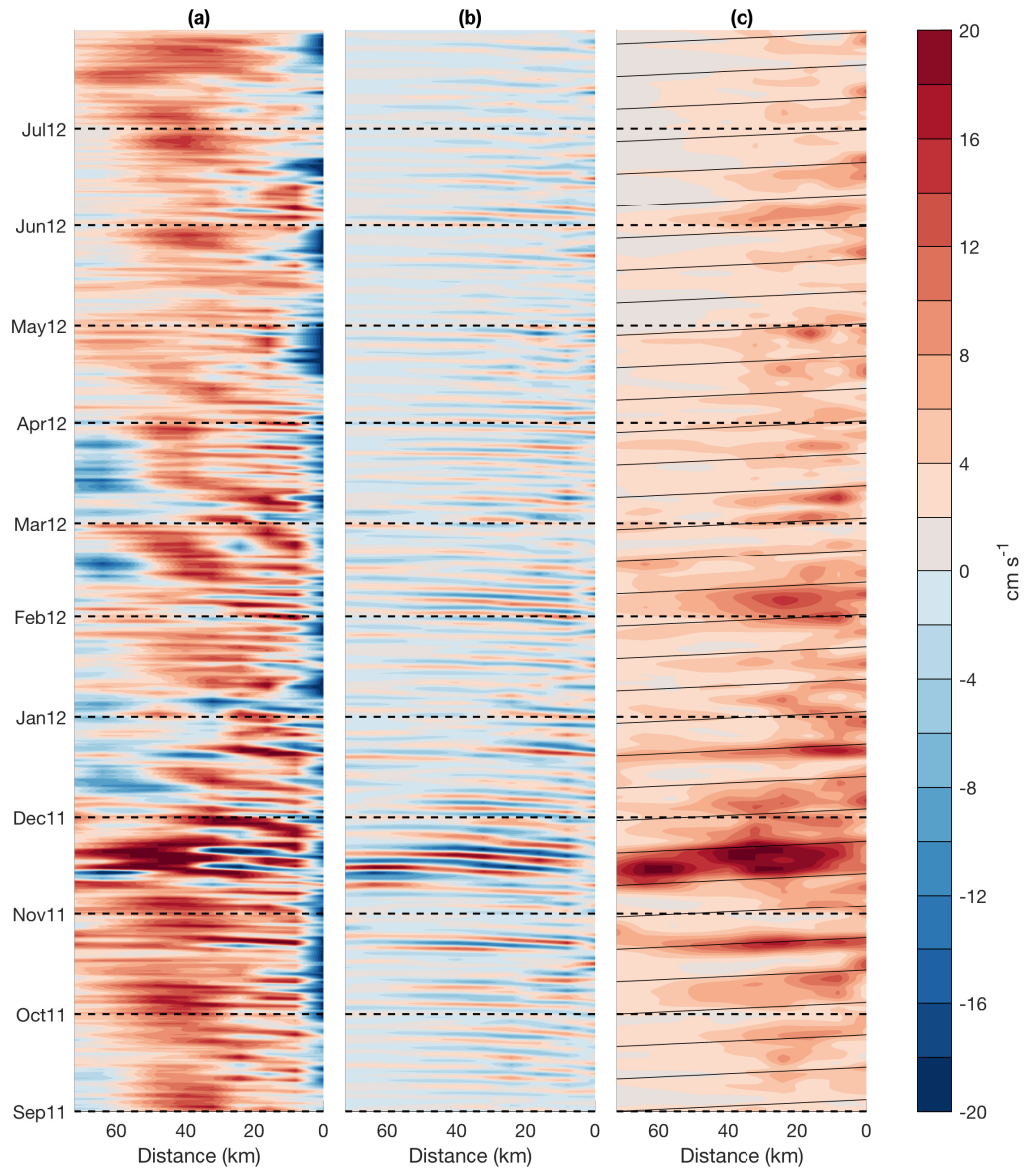


Figure 3: Hovmöller plots from the gridded mooring data of a) the depth-mean along-stream velocity (below 100 m, same for all plots); b) the 8-day high-passed, depth-mean component of velocity in the direction of the major axis of the local current ellipse; and c) the wavelet amplitude at a 4-day period for the depth-mean velocity. Iceland is to the right of each panel as in Figure 2. The wavelet analysis uses the jLab toolbox (Lilly, 2017) with standard Morlet wavelets with $\gamma=3$ and $\beta = 2$. The sloped, black guidelines in panel c are angled at the theoretical group velocity for the measured topographic Rossby waves (see text for details).

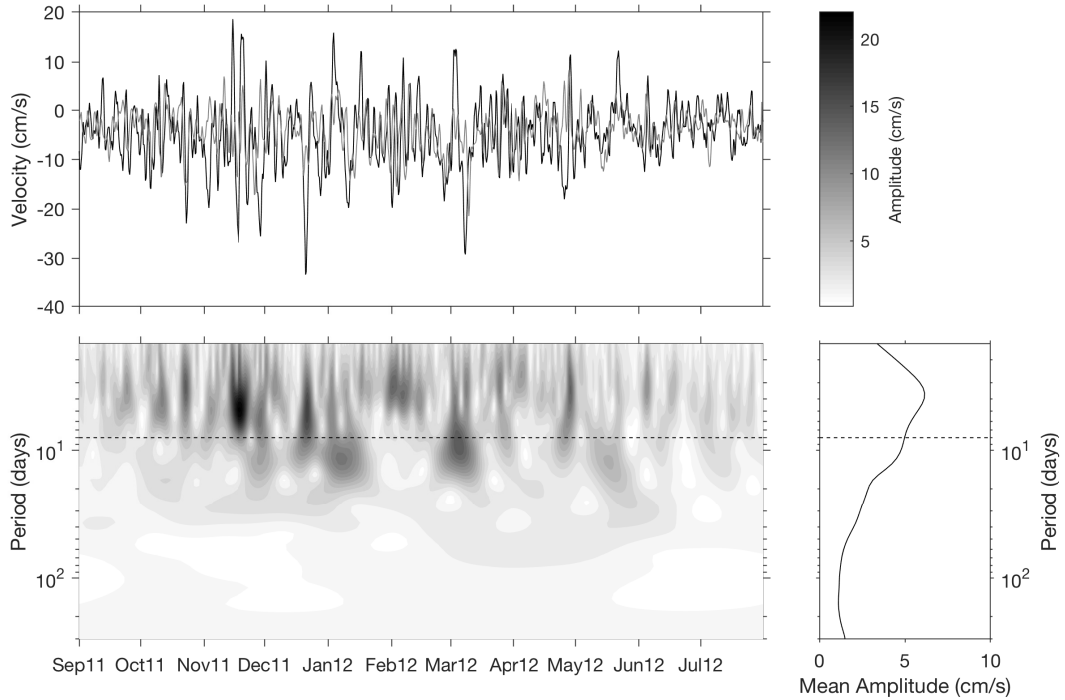


Figure 4: Top: Depth-averaged along-stream (black) and cross-stream (grey) components of velocity for the grid point closest to mooring KGA 3. Bottom left: Wavelet spectrum of the depth-averaged velocity using Morlet wavelets (Lilly, 2017). The color scale for this plot is at the top right. Bottom right: Mean wavelet amplitude for the length of the deployment. The dashed line in the bottom panels indicates the 8-day cut-off period for the high-pass filter used in this study.

155 characterizing different regimes across the array (Figure 5). In the NIIC (KGA 1), the
 156 current ellipse is elongated in the direction of the mean flow indicative of a current pulsing
 157 along its axis. By contrast, within the Separated EGC (KGA 6 and 7), the elongation of the
 158 current ellipses is perpendicular to the mean flow demonstrating that this current meanders.
 159 However, in the NIJ (KGA 2-4), the major axes of the current ellipses are aligned at an
 160 oblique angle to both the mean flow and the underlying bathymetry. KGA 5 appears to be
 161 in a transition region between conditions in the NIJ and those in the Separated EGC.

162 *a. Topographic Rossby Waves*

163 We resolved the sub-8-day depth-averaged flow in the gridded product along the major
 164 axis of the current ellipses at each offshore location. Particularly in the NIJ, the variability

165 along these axes have a sinusoidal form and are lagged between moorings such that the
 166 pulses of current progress offshore in time (Figure 3b). This implies a downslope phase
 167 propagation of this variability.

168 We argue that this is the signature of TRWs. These waves are supported by topo-
 169 graphic β and result in transverse fluctuations that are often at an oblique angle to the
 170 mean flow. TRWs are found in many slope regions of the worlds oceans (Garrett, 1979;
 171 Louis *et al.*, 1982; Pickart and Watts, 1990). Key features of TRWs include wave vec-
 172 tors (and hence phase velocities) that are perpendicular to the velocity variability, a group
 173 velocity which is at an oblique angle to the phase velocity, and a tendency to be bottom-
 174 trapped in regions of significant stratification.

175 Given that the phase propagation is perpendicular to the velocity variability, we de-
 176 duce that the wave phase is progressing downslope at -9°T (average from moorings KGA
 177 2–4, see Figure 5). Following Pickart and Watts (1990), we then calculated the phase
 178 speed over the range of moorings KGA 2–4 (where the wave signal is most pronounced)
 179 using,

$$c_p = \frac{1}{T} \frac{360}{\bar{\phi}} \frac{\overline{\Delta S}}{\cos(\Delta)}$$

180 where T is the wave period (= 3.6 days), $\bar{\phi}$ is the average phase offset (= $48 \pm 3^\circ$),
 181 $\overline{\Delta S}$ is the average instrument spacing (= 8.1 ± 0.2 km), and Δ is the angle between the
 182 mooring array and the direction of wave propagation (= $8 \pm 4^\circ$). The resulting phase
 183 speed is 17.3 ± 0.8 km day $^{-1}$ corresponding to a wavelength of 62 ± 3 km. The error
 184 estimates arise in equal contributions from uncertainties in $\bar{\phi}$, $\overline{\Delta S}$, and Δ .

185 As a consistency check that the observed fluctuations are in fact TRWs, we can em-
 186 ploy the TRW dispersion relation for a uniformly stratified ocean neglecting planetary β .
 187 Following Pedlosky (1979), this can be written as:

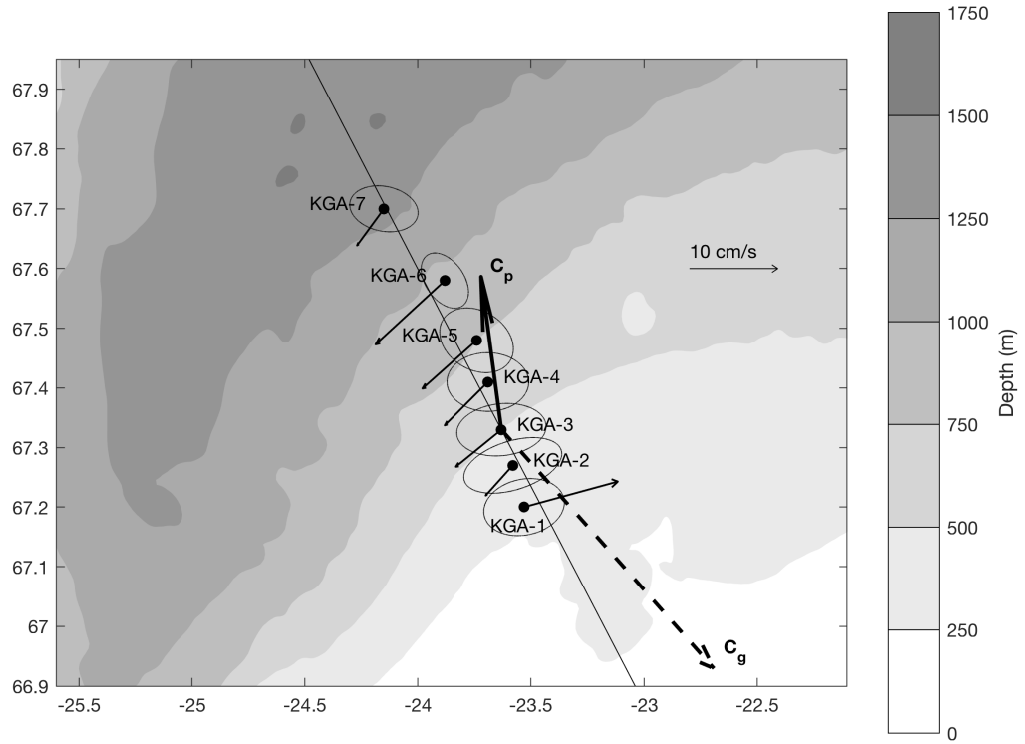


Figure 5: Aspects of the flow measured by the Kögur moorings (black circles). The thin vectors indicate the mean velocity averaged from 100 m to the depth of the ADCP at each mooring (see gray lines in Figure 2). Also shown are the 8-day high-passed current ellipses for the same depth range. The thick black arrow (C_p) denotes the direction of TRW phase propagation averaged over KGA 2-4 (plotted at KGA 3). The dashed black arrow shows the direction of TRW group velocity (C_g). All vectors and current ellipses are drawn to the same scale as indicated. The long black line is the mean downslope direction averaged between KGA 2-4. The bathymetry is from IBCAO v3.

$$T = \frac{2\pi \tanh\left(\frac{2\pi ND}{\lambda f}\right)}{N\Gamma \sin(\theta)}$$

188 where T is the period of the wave, N is the average water column Brunt Väisälä
 189 frequency ($= 3.3 \times 10^{-5}$, averaged using the gridded data below 100 m), D is the depth

190 (= 500 m), λ is the wavelength, f is the Coriolis parameter ($= 1.35 \times 10^{-4}$), Γ is the
191 bottom slope ($= 0.016$, from IBCAO v3), and θ is the phase velocity direction relative to
192 downslope.

193 We can test the predicted value of θ against the observed value using our knowledge
194 of the other variables. The predicted angle of 29° compares well with the measured value
195 of 24° (from the average downslope angle between moorings KGA 2–4). There is of
196 course uncertainty in the measured downslope angle depending on the region selected
197 for the averaging. For example, if we expand the calculation of the downslope direction
198 to encompass KGA 1–5, the measured θ becomes 33° , which still agrees well with the
199 predicted value. In addition, the bottom-trapping scale ($=f/Nk$) is much greater than
200 1000 m, in agreement with the observed velocities which are largely barotropic.

201 All of this supports our assertion that the dominant high-frequency variability in the
202 NIJ is due to TRWs. The obvious question is, where and how are these waves being
203 generated? Using the dispersion relation we can calculate the group velocity. For the
204 observed parameters, we find this to be 36 km day^{-1} directed almost directly up-slope at
205 the array site (138°T , see Figure 5). This implies that the energy source lies offshore.
206 We can corroborate this onshore propagation of energy observationally by considering the
207 wavelet amplitude for the 4-day signal at each mooring site. The Hovmöller plot of this
208 shows clear occurrences of onshore energy propagation that are in line with the predicted
209 group velocity (Figure 3c).

210 *b. Wave Tracing and TRW Formation Mechanisms*

211 In order to shed light on the source of the TRWs, we implemented the inverse wave
212 tracing model described in Section 2. In particular, we calculated the wave paths back-
213 wards in time from moorings KGA 2–5. For each mooring, the model was initialized
214 with the local wavenumber (assuming constant phase velocity and wave period). Since
215 KGA 5 only marginally displayed TRW behavior, the results from that mooring should
216 be considered less robust. The calculated paths indicate that the waves originate offshore

217 of the moorings in the vicinity of the deep Blossville Basin (Figure 6). While the traces
218 diverge somewhat going offshore, it is clear that they do not deflect significantly upstream
219 or downstream. In other words, the energy is not propagating along the Iceland continental
220 slope.

221 TRWs are a ubiquitous feature in the middle Atlantic Bight between Cape Hatteras,
222 NC and the Grand Banks (Louis *et al.*, 1982; Johns and Watts, 1986; Pickart and Watts,
223 1990). The source of the waves appears to be the Gulf Stream. Both Hogg (1981) and
224 Schultz (1987) argued that TRWs observed along the US continental slope emanated from
225 large amplitude Gulf Stream meanders offshore. Louis *et al.* (1982) made the case that
226 bursts of TRWs measured south of Nova Scotia resulted from Gulf Stream eddy formation.
227 Pickart (1995) demonstrated that the TRWs observed near Cape Hatteras were forced by
228 meanders of the Gulf Stream as it flowed over a bend in topography farther to the east.

229 In light of these studies, it is natural to suspect that the TRWs measured at the Kögur
230 array site are generated by the Separated EGC. This current is energetic, and, as noted
231 above, is subject to significant meandering (akin to the Gulf Stream). The wave tracing
232 indicates that the energy emanates from the Blossville Basin where the Separated EGC
233 resides. Additionally, there is evidence that times of strong TRW activity on the upper
234 slope are often preceded slightly by increases in meander energy offshore (Figure 3). The
235 high-energy event in November is one example of this, but there are additional instances
236 in late October, late December, and early March.

237 Another possible trigger for the waves is the intermittent aspiration of deeper waters
238 towards the Denmark Strait Sill. Harden *et al.* (2016) demonstrated that 0.6 Sv of the
239 overflow transport approaching the sill does so from below sill depth. Pulsing of this
240 aspirated component of the flow across the isobaths could initiate topographic wave activ-
241 ity. Regardless of the mechanism, the presence of TRWs raises the question of whether
242 they are present along the entire Iceland slope or whether they are unique to our sampling
243 region. To address this we examined the velocity data from a mooring deployed approxi-

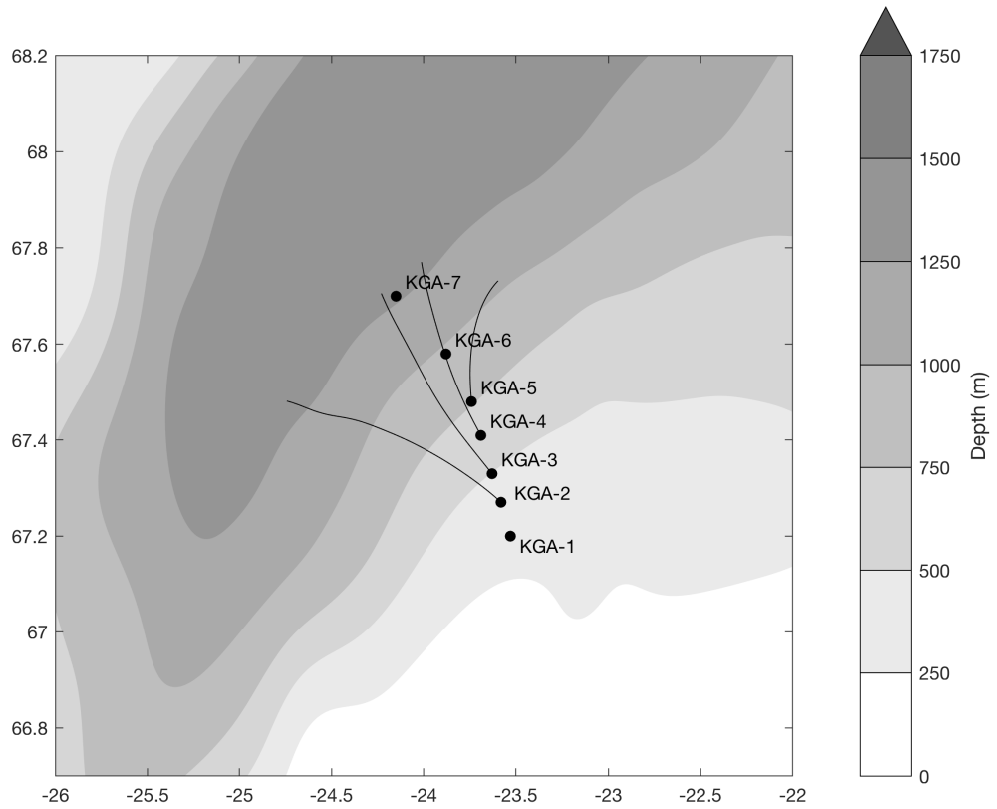


Figure 6: Paths of the Topographic Rossby Waves (thin lines) computed using the inverse wave tracing model for moorings KGA 2-5. Wave traces are truncated as they pass the 1500 m isobath. The bathymetry is from IBCAO v3 smoothed over 60 km (see text for details).

244 mately 200 km upstream on the Iceland slope near the Kolbeinsey ridge from 2007–2008
245 (Jónsson and Valdimarsson, 2012). The depth-mean velocity showed very little energy
246 in the 4-day period, at odds with the large TRW signal found at this period at the Kögur
247 array. Notably, the upstream mooring site is quite far from the Separated EGC (Figure 1)
248 and hence lacks that as an energy source.

249 **4. Summary and Discussion**

250 We have documented the existence of energetic topographic Rossby Waves (TRWs)
251 within the North Icelandic Jet (NIJ) using observations from the densely-instrumented
252 Kögur Array located approximately 200 km upstream of the Denmark Strait Sill. The
253 mean period of the waves is 3.6 days, the wavelength is 62 ± 3 km, and the phase velocity
254 is 17.3 ± 0.8 km day⁻¹ directed downslope (-9°T). Using the TRW dispersion relation,
255 we corroborated our observed direction of phase propagation relative to the downslope
256 direction (24°) with the theoretical value (29°). We further calculated that the wave energy
257 is progressing up-slope (138°T) at 36 km day⁻¹, in agreement with our observational
258 data. It is likely that the energy in the TRWs emanates locally near the mooring site,
259 either through the meandering of the offshore Separated East Greenland Current (EGC),
260 or through pulses of cross-bathymetric flow due to the aspiration of deep overflow water
261 as it approaches Denmark Strait.

262 Notably, our data imply that the dominant high-frequency variability at the Kögur site
263 does not originate from the Denmark Strait, nor does it propagate towards the sill. It sug-
264 gests that the mesoscale features at the sill (boluses and pulses), diagnosed observationally
265 by von Appen *et al.* (2017) and in a model framework by Almansi *et al.* (2017), are not
266 triggered by, nor excite, the TRWs on the Iceland Slope. However, the likelihood of a
267 connection between the high frequency variability at the two locations is still high given
268 the geographic proximity and the similarity in timescales, but is presumably mediated by
269 another process. The Denmark Strait overflow is believed to be subject to hydraulic con-

270 trol (Whitehead, 1998; Nikolopoulos *et al.*, 2003), and, consequently, information should
271 be transferred between the sill and the region to the north, likely as Kelvin waves. The ex-
272 istence of any such connection and the impact on both the sill and NIJ variability requires
273 further investigation and is the subject of an on-going study.

274 Finally, one also needs to consider where the energy in the TRWs ends up and what
275 impact it might have on the dynamics of the circulation inshore of the Iceland slope. The
276 energy likely cascades into the North Icelandic Irminger Current (NIIC) where it dissi-
277 pates, leading to enhanced mixing. It might also alter the stability of NIIC, which brings
278 warm subtropical water into the Nordic Seas. Våge *et al.* (2011) hypothesize that the off-
279 shore flux of this warm water associated with the disintegration of the NIIC is tied to the
280 overturning loop that forms the NIJ. Notably, eddies of NIIC water are found both in the
281 Blossville Basin (Jónsson and Valdimarsson, 2012) and farther north in the Iceland Sea
282 (Våge *et al.*, 2011). It is intriguing to think that the TRWs described here could play a role
283 in this aspect of the NIIC.

284 *Acknowledgments.* We would like to thank the crew and technicians aboard the R/V
285 Knorr and RSS James Clark Ross for the deployment and recovery of the Kögur moorings.
286 This work was supported by National Science Foundation grants OCE-1433958 (BH),
287 OCE-0959381 (BH and RP) and OCE-1558742 (RP).

288

289

REFERENCES

290 Almansi, M., T. W. N. Haine, R. S. Pickart, M. G. Magaldi, R. Gelderloos, and D. Mas-
291 tropole. 2017. High-Frequency Variability in the Circulation and Hydrography of the
292 Denmark Strait Overflow from a High-Resolution Numerical Model. *Journal of Physi-
293 cal Oceanography*, 47(12), 2999–3013. doi: 10.1175/JPO-D-17-0129.1.

- 294 Behrens, E., K. Våge, B. Harden, A. Biastoch, and C. W. Böning. 2017. Composition and
295 variability of the Denmark Strait Overflow Water in a high-resolution numerical model
296 hindcast simulation. *Journal of Geophysical Research: Oceans*, *122*(4), 2830–2846.
297 doi: 10.1002/2016JC012158.
- 298 Bruce, J. 1995. Eddies southwest of the Denmark Strait. *Deep Sea Research Part I:
299 Oceanographic Research Papers*, *42*(1), 13–29. doi: 10.1016/0967-0637(94)00040-Y.
- 300 Cooper, L. H. N. 1955. Deep water movements in the North Atlantic as a link between
301 climatic changes around Iceland and biological productivity of the English Channel and
302 Celtic Sea. *Journal of Marine Research*, *14*, 347–362.
- 303 Dickson, R. R. and J. Brown. 1994. The production of North Atlantic Deep Wa-
304 ter: Sources, rates, and pathways. *J. Geophys. Res.*, *99*, 12319–12341. doi:
305 10.1029/94JC00530.
- 306 Garrett, C. 1979. Topographic Rossby Waves off East Australia: Identification and Role in
307 Shelf Circulation. *Journal of Physical Oceanography*, *9*, 244–253. doi: 10.1175/1520-
308 0485(1979)009<0244:TRW0EA>2.0.CO;2.
- 309 Harden, B. E., R. S. Pickart, H. Valdimarsson, K. Våge, L. de Steur, C. Richards, F. Bahr,
310 D. Torres, E. Børve, S. Jónsson, A. Macrander, S. Østerhus, L. Håvik, and T. Hatter-
311 mann. 2016. Upstream sources of the Denmark Strait Overflow: Observations from
312 a high-resolution mooring array. *Deep Sea Research Part I: Oceanographic Research
313 Papers*, *112*, 94–112. doi: 10.1016/j.dsr.2016.02.007.
- 314 Håvik, L., K. Våge, R. S. Pickart, B. Harden, W. J. von Appen, S. Jónsson, and S. Øster-
315 hus. 2017. Structure and variability of the shelfbreak east greenland current north of
316 denmark strait. *Journal of Physical Oceanography*, *47*, 2631–2646. doi: 10.1175/JPO-
317 D-17-0062.1. URL <https://doi.org/10.1175/JPO-D-17-0062.1>.

318 Hogg, N. G. 1981. Topographic waves along 70°W on the continental rise. *Journal of*
319 *Marine Research*, *39*, 627–649.

320 Jakobsson, M., L. Mayer, B. Coakley, J. A. Dowdeswell, S. Forbes, B. Fridman, H. Hod-
321 nesdal, R. Noormets, R. Pedersen, M. Rebesco, H. W. Schenke, Y. Zarayskaya, D. Ac-
322 cettella, A. Armstrong, R. M. Anderson, P. Bienhoff, A. Camerlenghi, I. Church,
323 M. Edwards, J. V. Gardner, J. K. Hall, B. Hell, O. Hestvik, Y. Kristoffersen, C. Mar-
324 cussen, R. Mohammad, D. Mosher, S. V. Nghiem, M. T. Pedrosa, P. G. Travaglini, and
325 P. Weatherall. 2012. The International Bathymetric Chart of the Arctic Ocean (IBCAO)
326 Version 3.0. *Geophysical Research Letters*, *39*, L12609. doi: 10.1029/2012GL052219.

327 Jochumsen, K., M. Moritz, N. Nunes, D. Quadfasel, K. M. H. Larsen, B. Hansen,
328 H. Valdimarsson, and S. Jonsson. 2017. Revised transport estimates of the Den-
329 mark Strait overflow. *Journal of Geophysical Research: Oceans*, *122*, 3434–3450. doi:
330 10.1002/2017JC012803.

331 Johns, W. E. and D. R. Watts. 1986. Time scales and structure of topographic Rossby
332 waves and meanders in the deep Gulf Stream. *Journal of Marine Research*, *44*, 267–
333 290. doi: 10.1357/002224086788405356.

334 Jonsson, S. and H. Valdimarsson. February 2004. A new path for the denmark strait over-
335 flow water from the iceland sea to denmark strait. *Geophys. Res. Lett.*, *31*(3), L03305–.
336 ISSN 0094-8276. URL <http://dx.doi.org/10.1029/2003GL019214>.

337 Jónsson, S. and H. Valdimarsson. 2012. Hydrography and circulation over the southern
338 part of the Kolbeinsey Ridge. *ICES Journal of Marine Science: Journal du Conseil*.

339 Käse, R. H., J. B. Girton, and T. B. Sanford. 2003. Structure and variability of the
340 Denmark Strait Overflow: Model and observations. *Journal of Geophysical Research:*
341 *Oceans*, *108*, 3181. doi: 10.1029/2002JC001548.

342 Lilly, J. M. 2017. jLab: A data analysis package for Matlab, v 1.6.3.

- 343 Louis, J. P., B. D. Petrie, and P. C. Smith. 1982. Observations of topographic rossby
344 waves on the continental margin off nova scotia. *Journal of Physical Oceanography*, *12*,
345 47–55. doi: 10.1175/1520-0485(1982)012<0047:OOTRWO>2.0.CO;2.
- 346 Mastropole, D., R. S. Pickart, H. Valdimarsson, K. Våge, K. Jochumsen, and J. Gir-
347 ton. 2017. On the hydrography of Denmark Strait. *Journal of Geophysical Research:*
348 *Oceans*, *122*, 306–321. doi: 10.1002/2016JC012007.
- 349 Mauritzen, C. 1996. Production of dense overflow waters feeding the North Atlantic across
350 the Greenland-Scotland Ridge. Part 1: Evidence for a revised circulation scheme. *Deep*
351 *Sea Research Part I: Oceanographic Research Papers*, *43*, 769–806. doi: 10.1016/0967-
352 0637(96)00037-4.
- 353 Meinen, C., E. Fields, R. S. Pickart, and D. R. Watts. 1993. Ray tracing on topographic
354 rossby waves. Technical Report 93-1, University of Rhode Island.
- 355 Nikolopoulos, A., K. Borenäs, R. Hietala, and P. Lundberg. 2003. Hydraulic estimates of
356 Denmark Strait overflow. *Journal of Geophysical Research: Oceans*, *108*, 3095. doi:
357 10.1029/2001JC001283.
- 358 Pedlosky, J. 1979. *Geophysical Fluid Dynamics*. Springer US. doi: 10.1007/978-1-4684-
359 0071-7.
- 360 Pickart, R. S. 1995. Gulf Stream–Generated Topographic Rossby Waves.
361 *Journal of Physical Oceanography*, *25*, 574–586. doi: 10.1175/1520-
362 0485(1995)025<0574:GSTRW>2.0.CO;2.
- 363 Pickart, R. S. and D. R. Watts. 1990. Deep Western Boundary Current variability at Cape
364 Hatteras. *Journal of Marine Research*, *48*, 765–791.
- 365 Pickart, R. S., M. A. Spall, D. J. Torres, K. Våge, H. Valdimarsson, C. Nobre, G. W. K.
366 Moore, S. Jonsson, and D. Mastropole. 2017. The North Icelandic Jet and its relation-

367 ship to the North Icelandic Irminger Current. *Journal of Marine Research*, 75, 605–639.
368 doi: 10.1357/002224017822109505.

369 Rudels, B., E. Fahrbach, J. Meincke, G. Budéus, and P. Eriksson. 2002. The East Green-
370 land Current and its contribution to the Denmark Strait overflow. *ICES Journal of Ma-
371 rine Science: Journal du Conseil*, 59, 1133–1154. doi: 10.1006/jmsc.2002.1284.

372 Schultz, R. J., 1987. Structure and propagation of topographic rossby waves northeast of
373 cape hatteras, north carolina. Master's thesis, Marine Science Program, University of
374 North Carolina.

375 Smith, P. C. 1976. Baroclinic Instability in the Denmark Strait Overflow.
376 *J. Phys. Oceanogr.*, 6, 355–371. ISSN 0022-3670. doi: 10.1175/1520-
377 0485(1976)006<0355:BIITDS>2.0.CO;2.

378 Strass, V. H., E. Fahrbach, U. Schauer, and L. Sellmann. 1993. Formation of Denmark
379 Strait overflow water by mixing in the East Greenland Current. *Journal of Geophysical
380 Research: Oceans*, 98, 6907–6919. doi: 10.1029/92JC02732.

381 Våge, K., R. S. Pickart, M. A. Spall, H. Valdimarsson, S. Jónsson, D. J. Torres, S. Øster-
382 hus, and T. Eldevik. 2011. Significant role of the North Icelandic Jet in the formation
383 of Denmark Strait overflow water. *Nature Geosci*, 4, 723–727. ISSN 1752-0894. doi:
384 10.1038/ngeo1234.

385 Våge, K., R. S. Pickart, M. A. Spall, G. W. K. Moore, H. Valdimarsson, D. J. Torres, S. Y.
386 Erofeeva, and J. E. Ø. Nilsen. 2013. Revised circulation scheme north of the Denmark
387 Strait. *Deep Sea Research Part I: Oceanographic Research Papers*, 79, 20–39. doi:
388 10.1016/j.dsr.2013.05.007.

389 Våge, K., G. W. K. Moore, S. Jónsson, and H. Valdimarsson. 2015. Water mass transfor-
390 mation in the Iceland Sea. *Deep Sea Research Part I: Oceanographic Research Papers*,
391 101, 98–109. doi: 10.1016/j.dsr.2015.04.001.

- 392 von Appen, W. J., D. Mastropole, R. S. Pickart, H. Valdimarsson, S. Jónsson, and J. B.
393 Girton. 2017. On the nature of the mesoscale variability in denmark strait. *Journal of*
394 *Physical Oceanography*, 47, 567–582. doi: 10.1175/JPO-D-16-0127.1.
- 395 Whitehead, J. A. 1998. Topographic control of oceanic flows in deep passages and straits.
396 *Reviews of Geophysics*, 36, 423–440. doi: 10.1029/98RG01014.